22B.3 MRMS dual-polarization radar synthetic QPE

Jian Zhang[1], Lin Tang[1,2], Steve Cocks[1,2], Yadong Wang[1,2], Youcun Qi[1,2], Pengfei Zhang[1,2], Alexander Ryzhkov[1,2], Carrie Langston[1,2], Brian Kaney[1,2], and Kenneth Howard[1]

[1] NOAA/OAR/National Severe Storms Laboratory, Norman, OK

[2]Cooperative Institute for Mesoscale Meteorological Studies, University of Oklahoma, Norman, OK

1 INTRODUCTION

The National Weather Service Radar Operations Center implemented a near surface hydrometeor classification (HC, Park et al. 2009) and a Dual Pol (DP) radar quantitative precipitation estimation (QPE, Giangrande and Ryzhkov 2008) algorithm at each radar site with the completion of the DP upgrade to the WSR-88D network in 2013. The HC was based on the principles of fuzzy logics and membership functions utilizing DP variables. These advancements provided a much-improvement identification of non-hydrometeor returns over the single-polarization (SP) radar techniques. Subsequently the DP QPE had less contamination from anomalous propagation clutter and biological scatters than the precipitation process system (PPS, Fulton et al. 1998) used during the SP radar era. The DP QPE, based on reflectivity (Z), differential reflectivity (Zdr) and specific differential phase (Kdp), provided improved precipitation estimates (less mean bias) over SP PPS in some warm season events where the freezing level was elevated. However, it had relatively large random errors due to its high sensitivity to errors in Zdr in addition to discontinuities and biases in the QPE near the melting layer.

Studies utilizing specific attenuation, *A*, for radar-based QPEs (Ryzhkov et al. 2014; Wang et al. 2014) have shown immunity to calibration errors in Z and Zdr and the high linearity of R (rain rate) – A relationships. A is also immune to partial beam blockages. Kdp has similar advantages but the estimation of Kdp requires smoothing along the radial that degrades the spatial resolution. Conversely, *A* provides rain rate estimates at the native radar resolution in a wider range of rain intensities as opposed to Kdp which is very noisy in light rain. Based on these initial assessments, an alternative DP radar synthetic QPE approach was developed and tested within the Multi-Radar Multi-Sensor (MRMS, Zhang et al. 2016) system.

The MRMS DP QPE calculates R based on a combination of A, Kdp, and Z. While A has the aforementioned advantages for rain rate estimation, it is not applicable in radar observations that contain ice.

*Corresponding Author address: Jian Zhang, NSSL, 120 David L Boren Blvd, Norman, OK 73072; e-mail: jian.zhang@noaa.gov.

Therefore, the MRMS DP radar synthetic QPE applies R(A) relationship in areas where radar is observing pure rain, R(Kdp) in areas containing hail and a vertical profile corrected R(Z) elsewhere. The vertical profile correction is to account for reflectivity variations in and above the melting layer.

The MRMS DP synthetic QPE has been implemented in the real-time MRMS research system at NSSL CONUS wide since Oct. 2016 where extensive evaluations and a number of refinements were made. This paper provides an overview of the new technique and its performance for July - September of 2017, where R(A) was widely applied. Section 2 describes the main components of the new DP QPE, and section 4 presents evaluation results from CONUS. A summary follows in section 5.

2 METHODOLOGY

Figure 1 shows an overview flowchart of the MRMS DP synthetic QPE (also called "Q3DP"). The input data includes DP radar variables and environmental data such as 3D temperature, freezing level height and

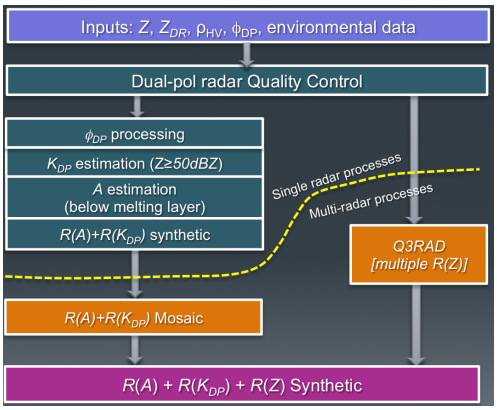

Fig. 1 An overview flowchart of the MRMS DP radar QPE.

surface wet bulb temperature. A DP radar quality control (Tang et al. 2014) is applied to remove non-precipitation echoes. After the QC, the differential phase, ϕ_{DP}, field is further processed for unfolding and smoothing. The Kdp is then calculated via a local linear fitting to ϕ_{DP} along the radial direction in areas where hail could be present (e.g., Z≥50dBZ). The specific attenuation, *A*, is calculated following the steps presented in Ryzhkov et al. (2014):

$$A(r) = \frac{Z_a^b(r)C(b,PIA)}{I(r_1,r_2) + C(b,PIA)I(r,r_2)} \quad (1)$$

Where:

$$I(r_1,r_2) = 0.46b\int_{r_1}^{r_2} Z_a^b(s)\,ds \quad (2)$$

$$I(r,r_2) = 0.46b\int_{r}^{r_2} Z_a^b(s)\,ds \quad (3)$$

$$C(b,PIA) = \exp(0.23bPIA) - 1 \quad (4)$$

$$PIA(r_1,r_2) = \alpha\left[\phi_{DP}(r_2) - \phi_{DP}(r_1)\right] \quad (5)$$

Here r is the range at a given gate, Z_a is the measured reflectivity, b is a constant (0.62 for S-band), PIA is the path-integrated attenuation and α is a parameter that generally varies with drop size distributions and with temperature (Ryzhkov et al. 2014). In the current scheme, α is estimated for each volume scan from the so-called Z/Zdr slope, K:

$$\alpha = -0.75K + 0.04875 \quad (6)$$

where K is the slope of a linear fit to the median Zdr values between 20–50 dBZ. Eq. (6) was obtained from the scattering simulations using disdrometer data and supported by analysis of ~10 events with relatively wide spread moderate to heavy precipitation events from different geographical regimes. Figure 2 shows Z (Figs. 2a, and 2d), Zdr (Figs. 2b and 2e) fields from the 0.5° tilt and the associated Z-Zdr scatter plots (Figs. 2c and 2f). For each 2-dBZ reflectivity bin a median Zdr value (black dots in Figs. 2c and 2f) was found and a linear fit (white dashed line) was made to the median Zdr values. The slope of the linear fit, K (Figs.2c and 2f), is then

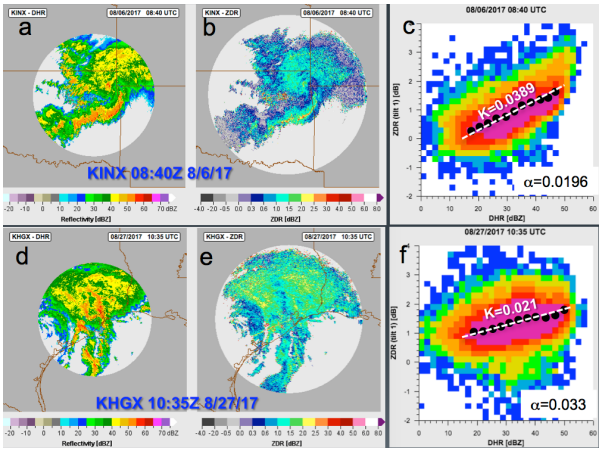

Fig. 2 The 0.5° tilt Z (a,d) and Zdr (b,e) fields from KINX (a,b) and KHGX (d,e) from a mesoscale convective system (a,b) and Hurricane Harvey (d, e). The corresponding Z/Zdr plots are shown in c and f, respectively, where the black dots indicate median Zdr values and white dashed lines represent the linear fit to the median Zdr vs Z.

used to calculate α. For the mesoscale convective system (Fig.2c), there was an apparent increase of Zdr with increasing Z, indicating the presence of large droplets in the convective system. As a result the Z/Zdr slope was relatively steep (K=0.0389 dB/dBZ) and α value (0.0196) was close to one of those for convective rain (Ryzhkov et al. 2014). For the Hurricane Harvey (Fig.2f), the Z-Zdr slope was relatively flat (K=0.021) and α (0.0347) was close to a tropical rain type value. When the precipitation is sporadic or is pure stratiform, there may not be not enough Z-Zdr pairs in the 20-50 dBZ range. Under these circumstances, a stratiform rain check is performed. If significant number of pairs exists in the 10-30 dBZ range, then the precipitation is considered pure stratiform and a default stratiform α (0.035) is applied. Otherwise either a new linear fit is applied to 10-40dBZ range (if sufficient data were found) or the precipitation is considered sporadic and a default convective α (0.015) is applied.

It is noted that R(A) is only applicable in radar observation areas that are free of ice. Within MRMS, the Z-Zdr data for α estimation are collected below the bottom of the melting layer. The melting layer bottom is determined from model temperature soundings and the correlation coefficient (ρ_{hv}) field. The specific attenuation, A, is only calculated below the melting layer.

Precipitation rates are estimated for individual radars from A (if Z < 50dBZ) or Kdp (Z ≥ 50dBZ) based on the following equations:

$$R(A) = 4120A^{1.03} \quad (7)$$

$$R(K_{DP}) = 29.0\,|K_{DP}^{0.77}| \quad (8)$$

Here the R(A) relationship is for S-band at 20°C (Ryzhkov et al. 2014), and the R(Kdp) relation was derived using disdrometer measurements in rain observed in the proximity of hailstorms in central Oklahoma.

Although the intercept in the R(A) relationship and parameter α are in general the functions of temperature, a single R(A) relation determined by Eq. (7) is used on the whole operational network of the WSR-88D radars. This is because that the estimate of rain rate from A is proportional to the product of the intercept and parameter α at S band (Ryzhkov et al. 2014). The intercept increases with temperature and the factor α decreases with temperature in the same proportion, so that their product remains almost unchanged and the temperature dependence can be ignored. This is confirmed by the low sensitivity of the R(A) performance to different temperatures in the multitude of WSR-88D observations in different areas of CONUS.

Precipitation rate fields from individual radars are mosaicked through a physically based scheme shown in Qi and Zhang (2017). Since R(A) is only valid below the melting layer, the R(A) and R(Kdp) mosaic has data voids in areas far away from the radars (e.g., the wedge in the southern Mississippi; Fig.3a). In the MRMS DP synthetic QPE, a multiple R(Z) QPE ("Q3RAD" Fig.3b) based on automated precipitation classifications and a vertical profile of reflectivity correction (Zhang et al. 2016) is used to fill in the voids. To prevent discontinuities between R(A) and R(Z), a weighted mean of the two rates is applied in a 50km transition zone near the outer boundary of R(A) (yellow colored area in Fig.3c). The MRMS DP synthetic QPE produced significantly higher rain rates in areas near southeastern Louisiana (Fig. 3a) than the R(Z) based QPE (Fig. 3b). And the higher rain rates resulted in a 24-hr accumulation that compared better with gauge observations (Figs. 4a vs. 4b).

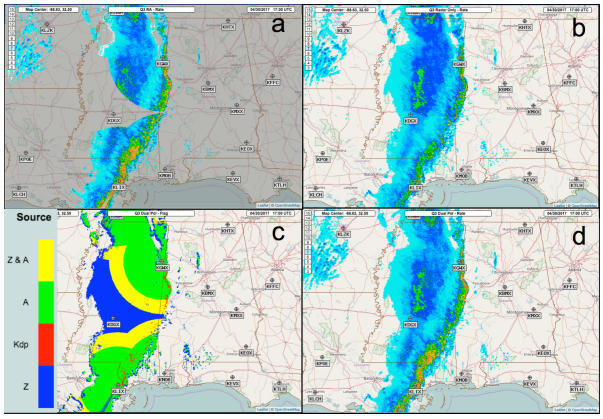

Fig. 3 Precipitation rate fields from the mosaic of R(A)+R(Kdp) (a) and multiple R(Z) (b) and the final synthetic QPE (d). Panel c shows a category field that indicates how the rate at each grid box was obtained. The data was valid at 17Z on 30 April 2017.

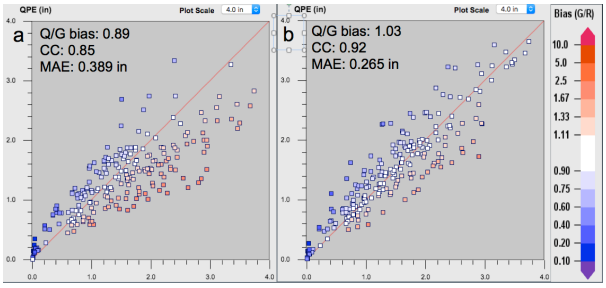

Fig. 4 Scatter plots of 24hr QPE accumulations from the multiple R(Z) (a) and the DP synthetic (b) versus gauges. The accumulation period ended at 12Z on 1 May 2017. The bubbles in a and b indicate locations of gauges. The statistic scores denoted in the scatter plots (c and d) are bias ratio, correlation coefficient (CC) and mean absolute error (MAE).

3 EVALUATIONS

The MRMS DP synthetic QPE has been tested and refined in the real-time MRMS research system at NSSL since Oct. 2016. Since R(A) uses the Zdr-Z slope and the radial profile of Z instead of their absolute values, it is immune to calibration errors of Z and Zdr. Figure 5 shows example 24hr rainfall accumulations from R(Z,Zdr) and R(A) QPEs from KCAE (Columbia, SC) radar ending at 11Z on 4 Oct. 2015. The partial blockages due to trees northwest of the radar was apparent in the R(Z,Zdr) QPE (Fig.5a). The blockages are largely mitigated in the R(A) QPE (Fig.5b) and the rainfall accumulation is much more continuous and agreed better with the gauges (Fig. 5d) than the R(Z,Zdr) QPE (Fig.5c).

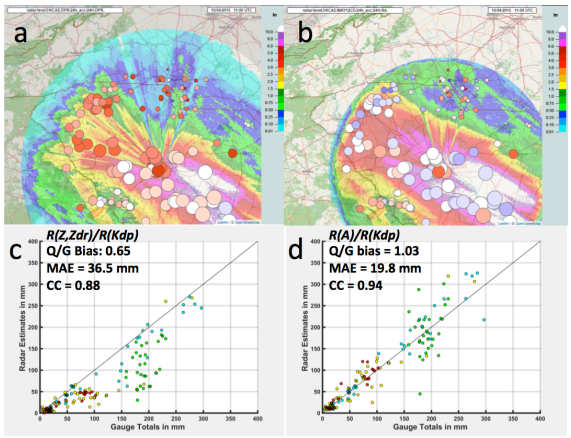

Fig. 5 Rainfall maps (color-shaded) from the R(Z, Zdr)/R(Kdp) (a) and the new R(A)/R(Kdp)/R(Z) synthetic (b) QPEs and their comparisons with gauges (c and d). The bubbles in a and b indicate locations of gauges. The size of the bubbles represents the gauge amounts and the color represents the bias ratio of gauge over QPE (pink-red colors indicating QPE underestimation and blue-purple indicating overestimation). The data is for 24hr accumulations ending at 11Z on 4 Oct. 2015. The color of the dots in c and d represents different distances of the gauges from the radar.

Figure 6 shows statistics of three NWS operational radar QPEs and the latest Q3DP from four radars in Texas (KHGX, KEWX, KGRK) and Louisiana (KLCH) during the Hurricane Harvey (Table 1). The three operational QPEs are Precipitation Processing System (PPS, Fulton et al. 1998), the hydrometeor classification-based R(Z,Zdr)/R(Kdp)/R(Z) synthetic QPE called Digital Precipitation Rate (DPR, Giangrande and Ryzhkov 2008) and the MRMS multiple R(Z) QPE ("Q3RAD", Zhang et al. 2016) based on precipitation classifications. PPS and DPR are single radar QPEs and Q3RAD a multi-radar mosaicked QPE. During this time period, PPS was primarily set to the tropical Z-R relationship below:

$$R = 250Z^{1.2} \quad (9)$$

And the DPR was mostly based on:

$$R(Z, Zdr) = 0.007Z^{0.927}Zdr^{-3.43} \quad (10)$$

$$R(Kdp) = 44.0\ |Kdp|^{0.822}\ sign\ (Kdp) \qquad (11)$$

Table 1 List of events during the Hurricane Harvey

ID	Radar/Date	ID	Radar/Date	ID	Radar/Date
1	KHGX 8/25-8/26/17	6	KGRK 8/26-8/27/17	11	KLCH 8/27-8/28/17
2	KEWX 8/25-8/26/17	7	KLCH 8/26-8/27/17	12	KHGX 8/28-8/29/17
3	KGRK 8/25-8/26/17	8	KHGX 8/27-8/28/17	13	KLCH 8/28-8/29/17
4	KHGX 8/26-8/27/17	9	KEWX 8/27-8/28/17	14	KHGX 8/29-8/30/17
5	KEWX 8/26-8/27/17	10	KGRK 8/27-8/28/17	15	KLCH 8/29-8/30/17

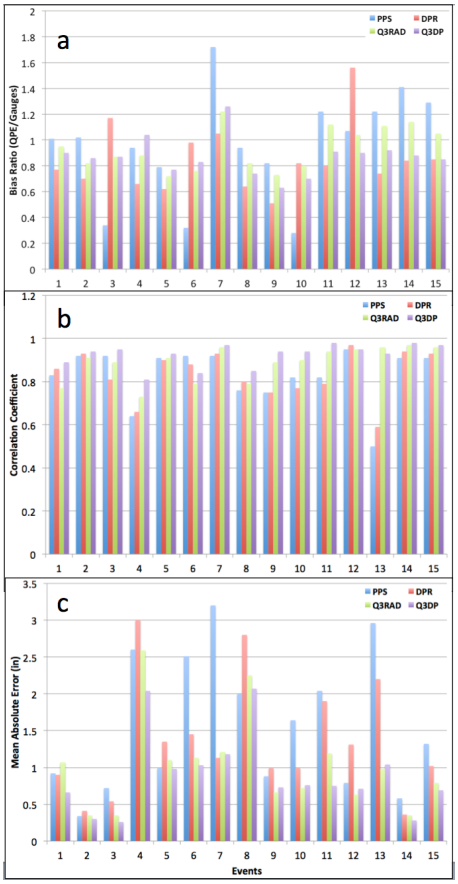

Fig. 6 The bias ratio (a), correlation coefficient (b) and mean absolute error (c) of three operational QPEs (PPS, DPR, Q3RAD) and the new MRMS DP synthetic QPE when compared with quality controlled hourly and daily gauges. The time and location of each event is shown in Table 1.

The new DP QPE (purple bars, Fig.6) had the least bias, MAE and highest CC among majority of the events, while PPS (blue) and DPR (red) had relatively large variations in the three scores. The reductions of MAE with respect to PPS are 6.3% in DPR, 16.7% in Q3RAD, and 20.5% in Q3DP. PPS had severe underestimations for three events (#3, #6, #10, Fig.6a) and all three were from KGRK radar that was roughly 4dBZ cooler than its neighboring radars. PPS also had significant overestimation biases for five events, (#7, 11, 13, 14 and 15). All these events except #14 were from KLCH which was ~1.1dBZ hotter. Q3RAD, while also based on R(Z) relationships, had less biases than PPS for the KGRK and KLCH events. This was due to the fact that 1) a spatially varying R(Z) was applied in Q3RAD based on precipitation classification and 2) neighboring radars that did not have a calibration issue contributed to the mosaicked QPE. For instance, the precipitation during event #7 around KLCH was largely convective thus Q3RAD applied a convective instead of tropical R(Z) for a large portion of the period, while PPS applied the tropical R(Z) for the whole period.

DPR had a lower bias than PPS although its MAE remained large relatively large (Fig.6c). The relatively large random errors in DPR were due to its high sensitivity to Zdr variations (Eq. [10]). Obtaining high-precision Zdr measurements remains a hardware engineering challenge; hence the applications of DPR may be limited at the current time.

Q3DP, by avoiding the direct use of absolute Z and Zdr values, showed a better performance than DPR for most of the events when compared with gauges. However, for event #9 (KEWX 8/27-8/28), a large underestimation bias (~37%) was found. A closer look at the KEWX data revealed suspicious negative Zdr data in some azimuths but not in others. The bad data was due to a hardware problem related to the azimuth rotary joint of the radar. The unevenly distributed bad Zdr data resulted in an unpresentative Z-Zdr distribution and subsequently inaccurate (low) α. The bad KEWX data was also contributed to the underestimation in Q3DP for events #8 (KHGX) and 10 (KGRK) due to the mosaicking process.

A larger scale evaluation of the MRMS DP synthetic QPE ("Q3DP") was carried out for 166 events (Table 2) across CONUS during Jul-Sep 2017. These events encompass mesoscale convective systems, hurricanes (Harvey and Irma), wide spread stratiform rains in the east and northeast, scattered convective storms in the semi-arid regions of the southwest, etc. The two QPEs were compared with quality controlled hourly MADIS (Meteorological Assimilation Data Ingest System; madis.noaa.gov) and daily CoCoRaHS (Community Collaborative Rain, Hail & Snow Network, https://www.cocorahs.org/) gauges. Figure 7a shows the domain average QPE/gauge bias ratios subtracted by 1.05 (assuming an average of 5% gauge under catch) for the two QPEs. The values above (under) the zero line indicate overestimation (underestimation) and the further above (below) the value from the zero line, the worse the over-(under-)estimation. The Q3RAD had more events with wet biases than with dry biases (Fig.7a). The events with significant wet biases (see black asterisks in Table 2 and black notations in Fig.7a) were from the southwest (AZ, NM, NV, UT), the Rocky

Mountains (CO, WY) and the northern US (NE, SD, ND), where the atmospheric environment was relatively dry. The domain averaged daily rainfall for these events were mostly below 0.25 in and the maximum rainfall below 2.5 in (Table 3), indicating light or moderate rain. An examination of the rainfall maps (not shown) revealed mostly scattered nature of these events. Therefore evaporation was mostly likely a main contributor to the overestimation. An evaporation correction scheme is currently under testing and was found to further mitigate the wet biases.

Table 2 List of events for the evaluation of the new DP QPE

eventID	Location/Time	eventID	Location/Time	eventID	Location/Time	eventID	Location/Time
1	KGLD KS 7-13	43	Upper Ohio Valley 7-28	85	WY-CO-NE-SD 8-15★	127	CO-NE-SD 9-1 ★★
2	Northctral 7-13	44	North central 7-28	86	AR-TN-MS 8-15	128	Northern plains 9-2
3	KAMX FL 7-13 ★★	45	Rockies/AZ 7-29	87	NC-VA-MD 8-16	129	KY-TN-OH 9-2 ★★
4	Northeast 7-14	46	Southeast 7-29	88	OK-AR-LA-MS-AL US 8-16	130	East coast 9-2
5	AZ-NM 7-16	47	Upper Atlantic 7-29	89	Nebraska 8-16	131	FL 9-2
6	Southeast 7-16	48	Rockies/SW 7-30	90	MN 8-17	132	FL 9-3
7	CO 7-16	49	Southeast 7-30	91	OK/MO 8-17	133	Northeast 9-3
8	Southwest 7-17	50	FL 7-31	92	OK-KS-NE-SD 8-18★	134	Great Lakes 9-3
9	Southeast 7-17	51	Southwest/Rockies 7-31	93	IN-OH-WV-TN 8-18	135	Great Lakes 9-4
10	Southwest 7-18	52	Northern US 8-3	94	WV-MD-northeast 8-19	136	Southeast 9-6
11	SD-ND-MN 7-18	53	Gulf Coast 8-3	95	Northeast 8-20	137	Northeast 9-6
12	NE 7-18	54	FL-SC 8-3	96	NE/IA 8-20	138	Carolinas 9-6 ★
13	Northeast 7-18	55	Gulf Coast 8-4	97	NM 8-21	139	East Coast 9-7
14	Southeast 7-18	56	Great Lakes 8-4	98	IA 8-21 ★	140	Great Lakes 9-8
15	AZ-NM 7-18	57	OK-KS-MO 8-6 ★	99	Upper Midwest 8-22	141	Southwest 9-9
16	Upper Midwest 7-19	58	Eastern US 8-7	100	OK-TX 8-23	142	FL 9-10 ★★
17	Southwest 7-19	59	OK-TX 8-7	101	TN-WV-IN-OH-PA 8-23	143	FL 9-11
18	Southeast 7-19	60	UT-CO-NM 8-7	102	SC-NC-VA 8-24	144	AL-GA-SC 9-12★★★
19	WY-CO-NE 7-20★	61	CO-NM-TX 8-8 ★	103	AZ-NM 8-24★★	145	AR-MS-TN-KY 9-13★★
20	SD-MN-WI 7-20	62	Easter/SE US 8-8	104	FL 8-25	146	NC 9-13 ★★
21	Southwest 7-20	63	Gulf Coast 8-8	105	NE-SD-MN 8-26	147	MT-ID-WY 9-15
22	AZ-NM-UT-CO 7-21	64	Northern US NW 8-9	106	South TX 8-26	148	UT-CO 9-15
23	WY-SD-ND 7-21 ★	65	Southeast 8-9	107	FL 8-26	149	Northern US 9-16
24	IL-IN-PA-NY 7-21	66	OK-KS 8-10	108	FL 8-27	150	KS-IA-MN 9-17
25	Upper Midwest 7-22	67	Southeast 8-10	109	MN-WI 8-27	151	Pacific NW 9-18★
26	AZ-NM-UT-CO 7-22★	68	CO/WY 8-10	110	NE-SD 8-27	152	Midwest 9-18
27	PA-VA-WV-OH-KY 7-23	69	MN 8-10	111	TX 8-27	153	Pacific NW 9-19
28	KS-MO-IL-IN 7-23	70	WI-IL-IA 8-11	112	KS-MO-IL-WI 8-28	154	MT-ID-WY 9-19
29	Southeast 7-23	71	OK-KS-MO 8-11	113	TX 8-28★	155	Upper Midwest 9-19
30	Southwest 7-23	72	LA-MS-AL 8-11	114	FL 8-28	156	Pacific NW 9-20
31	OH-PA-NY 7-24	73	AZ-NM-CO 8-11	115	TX-LA 8-29	157	ND-MN 9-20
32	Mid-Atlantic 7-24	74	LA-AR-TN 8-12	116	FL 8-29	158	IA-WI 9-21
33	OK-AR-LA 7-24	75	PA-MD-NJ 8-12	117	WI-IL-IN-OH-MI-WV 8-29	159	Pacific NW 9-21
34	NV-AZ-NM 7-24	76	SC-NC 8-12	118	SC-NC-VA 8-29	160	ID-NV-UT 9-22
35	NV-UT-AZ-CO 7-25	77	NM-CO-TX 8-12	119	Northeast 8-30★	161	MN-WI 9-23
36	Gulf/Southeast 7-25	78	OK 8-13	120	Gulf 8-30	162	MT-WY 9-23
37	Northeast 7-25	79	AZ 8-13	121	Southeast 8-31	163	Central US 9-24
38	Southwest 7-26	80	TN-NC-VA-WV 8-13	122	WI 8-31	164	Central US 9-25
39	Midwest 7-26	81	CO-NE-SD-ND 8-13	123	NV-UT 8-31★	165	Central US 9-26
40	Southeast 7-26	82	CO-NE-SD-ND 8-14	124	Southeast 9-1	166	TX-OK 9-27
41	Midwest 7-27	83	OK-TX-MO 8-14	125	AR-TN-KY 9-1		
42	AZ/NM 7-28 ★	84	GA-SC-NC 8-15	126	Eastern US 9-1		

NOTE: black asterisks in Table 2 indicate events with significant overestimation biases compared with gauges; red asterisks indicate events with large biases in Q3DP than in Q3RAD; blue asterisks indicate lower CC and green asterisks higher MAE in Q3DP than in Q3RAD.

Table 3 List of events with significant wet bias in Q3DP

Events	19	23	26	42	85
Gmean (in)	0.18	0.15	0.2	0.11	0.17
Gmax (in)	2.31	2.07	2.78	2.46	2.73
# of gauges	731	712	1871	485	749
Events	92	98	103	123	127
Gmean (in)	0.17	0.38	0.28	0.08	0.09
Gmax (in)	2.58	2.44	3.08	0.88	0.8
# of gauges	651	109	606	198	524

Figure 7b and 7c show the correlation coefficient and mean absolute error differences between Q3RAD and Q3DP with respect to gauges. The positive (negative) values in Fig. 7b indicate higher (lower) CC in Q3DP than Q3RAD, and the positive (negative) values in Fig. 7c indicate smaller (greater) MAE in Q3DP than in Q3RAD. The Q3DP performed better than Q3RAD in most of the events, while there are a handful of events where Q3DP performed worse. Further investigations were carried out on those events and initial analysis results were summarized below.

a) Q3DP with larger overestimation bias

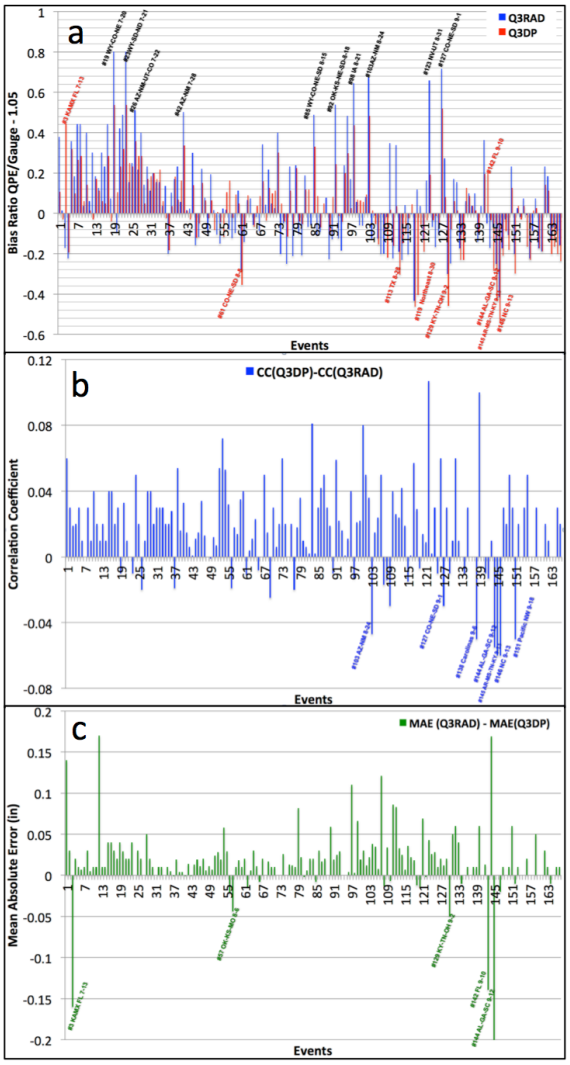

Fig. 7 The bias ratios of Q3RAD (blue) and Q3DP (red) versus gauges subtracted by 1.05 (a). Positive (negative) values indicate over-(under-)estimations. Panels b and c show the correlation coefficient (b) and mean absolute error (c) differences between Q3RAD and Q3DP. Positive (negative) values indicate higher (lower) CCs (b) and smaller (larger) MAEs in Q3DP. Interesting events where Q3DP had a performance issue were denoted in each panels and detailed discussions can be found in the text. The time and location of each event is shown in Table 2.

Q3DP had larger wet biases than Q3RAD for events #3 (KAMX, FL 7-13) and 142 (FL 9-10). Both events had a mixed convective and stratiform rain with large areas being stratiform. Figure 8 shows the 24hr rainfall maps of Q3RAD and Q3DP compared with the gauges for the FL 7-13 event. The overestimation in Q3DP occurred in areas along the east coast between KAMX and KMLB (Fig.8b). The α values varied from 0.019 at the beginning of the event at ~16Z 7/12 and increased to 0.03 around 22:35Z. It then stayed at 0.033-0.035 for the rest of the event and resulted in the largest overestimation between 22Z 7/12 and 03Z 7/13/2017. The MRMS hybrid scan reflectivity and precipitation type

(Figs. 8c and 8d) indicated a mixed convective and tropical rain in the region. However, the large area of stratiform rain to the west may have contributed to the large α, which was applied in the whole radar domain and resulted in overestimation in the convective rain band to the east. A next step is to segregate convective and stratiform areas for such events and apply different α values. The FL 9-10 event had similar characteristics with mixed tropical and convective rains, in addition to the potentially severe gauge undercatch due to strong winds during the Hurricane Irma.

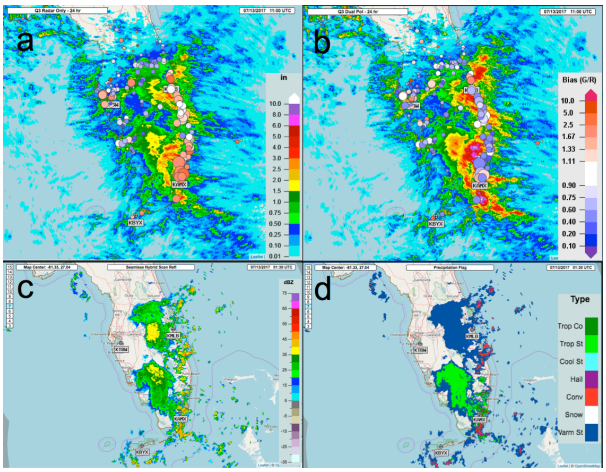

Fig. 8 Rainfall maps (color-shaded) from Q3RAD (a) and Q3DP (b) and their comparisons with gauges. The bubbles in a and b indicate gauge location/amounts and QPE/G biases the same way as in Fig.5. The data is for 24hr accumulations ending at 11Z on 13 Jul. 2017. Panel c shows the MRMS seamless hybrid scan reflectivity and panel d shows the precipitation type field.

b) Q3DP underestimation bias events

Q3DP had larger underestimation biases than Q3RAD for seven events (Table 4), three of which are light rain events (61, 145, and 146) with domain mean (max) 24hr gauge rainfall less than 0.4 in (3 in). Both Q3RAD and Q3DP had underestimation for the three events, while R(A) underestimation was more severe. This poorer performance of R(A) at light rain was likely due to a small $\Delta\phi_{DP}$ span criteria (> 0°) for R(A) applications in the MRMS DP QPE. This criteria may need to be adjusted to a higher value (e.g., 2°) for a more robust R(A) performance.

Table 4 List of events with larger underestimaion in Q3DP than in Q3RAD

Events	61	113	119	129	144	145	146
Gmean (in)	0.37	2.2	0.43	0.76	1.88	0.2	0.3
Gmax (in)	2.96	18.35	5.45	4.33	8.64	1.1	3.26
# of gauges	836	750	1005	372	1082	598	376

Two of the seven events (113 and 144) were found to have an azimuth rotary joint issue as discussed before. The radars involved were KEWX (113) and KFFC (144). The last two events (119 and 129) are both wide spread stratiform rain with relatively low intensities. Figure 9 shows example hourly Q3RAD and Q3DP QPEs (Figs. 9a and 9b) ending at 04Z on 9/2/17 from event 119 where Q3DP had a distinct underestimation. Figures 9c and 9d shows the base reflectivity and ϕ_{DP} fields at 03:30Z on 9/2/17. While the radar fields showed a typical stratiform rain, the Z-Zdr distribution between 10-40dBZ had a relatively steep slope and resulted in a low α value of 0.0155 (Fig. 9e). Same issues were found for event 129 (not shown). To mitigate the underestimation, a more robust stratiform rain check should be applied to avoid a Z-Zdr fitting to light rain.

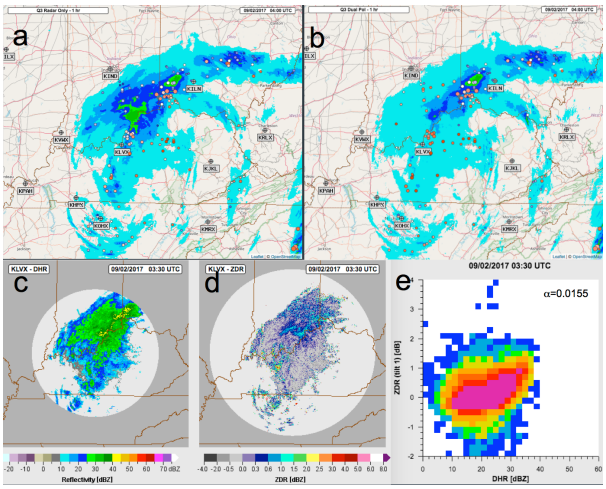

Fig. 9 Rainfall maps (color-shaded) from Q3RAD (a) and Q3DP (b) and their comparisons with gauges. The data is for 1hr accumulations ending at 04Z on 2 Sep. 2017. Panel c and d show the base Z and Zdr fields, respectively and panel e shows the corresponding Z-Zdr scatterplot.

c) Q3DP low CC events

Q3DP had lower CC than Q3RAD for seven events (Table 5), all of which except for one (#144) are light rain events with domain mean (max) 24hr gauge rainfall less than 0.4 in (3 in). These results again may indicate a need to adjust the $\Delta\phi_{DP}$ criteria from 0° to a higher value.

Table 5 List of events with lower CC in Q3DP than in Q3RAD

Events	103	127	138	144	145	146	151
Gmean (in)	0.28	0.09	0.53	1.88	0.2	0.3	0.26
Gmax (in)	3.08	0.8	2.8	8.64	1.1	3.26	1.78
# of gauges	606	524	295	1082	598	376	328

d) Q3DP large MAE events

Q3DP had higher MAE than Q3RAD for five events (Table 6), four of which (3, 129, 142, and 144) were discussed earlier. The event #57 (OK-KS-MO-8-6) was

a mesoscale convective system with a mixed convective and stratiform rain. During the hours when Q3DP had significant overestimation (e.g., 06-08Z 8/6/17 near KINX), the large stratiform rain areas behind the leading convective line resulted in a α value of 0.026 ~ 0.034. These high α values, when applied in the convective rain, would cause overestimation. A refined R(A) scheme with segregated convective and stratiform rain and corresponding α parameters may mitigate such overestimation.

Table 6 List of events with higher MAE in Q3DP than in Q3RAD

Events	3	57	129	142	144
Gmean (in)	0.8	1.08	0.76	1.27	1.88
Gmax (in)	5.05	8.5	4.33	7.59	8.64
# of gauges	211	1009	372	184	1082

4 SUMMARY

A new dual-pol radar synthetic QPE was developed in the MRMS system for improved accuracy of precipitation estimation. The new QPE was based on the specific attenuation A, the specific differential phase Kdp, and reflectivity Z. The advantages of the new DP QPE include: 1) immunity to partial beam blockages; 2) immune to calibration errors in Z and Zdr; and 3) higher spatial resolution than R(Kdp). The new DP QPE showed superior performance when compared with three current NWS operational radar QPEs for Hurricane Harvey, demonstrating its immunity to calibration errors in Z and Zdr fields. The new DP QPE was also evaluated for 166 events during Jul-Sep 2017 across CONUS and showed advantages over a multiple R(Z) based QPE, especially for moderate to heavy rains. The new DP QPE is planned for transition into the operational MRMS system in 2018.

References

Fulton, R., J. Breidenbach, D.-J. Seo, D. Miller, and T. O'Bannon, 1998: The WSR-88D rainfall algorithm. Wea. Forecasting, 13, 377–395.

Giangrande, Scott E., Alexander V. Ryzhkov, 2008: Estimation of rainfall based on the results of polarimetric echo classification. J. Appl. Meteor. Climatol., 47, 2445–2462.

Park, H.S., , A. V. Ryzhkov, D. S. Zrnić, and Kyung-Eak Kim, 2009: The Hydrometeor Classification Algorithm for the Polarimetric WSR-88D: Description and Application to an MCS. Weather and Forecasting. 24, 730-748.

Ryzhkov, Z., M. Diederich, P. Zhang, C. Simmer, 2014: Potential utilization of specific attenuation for rainfall estimation, mitigation of partial beam blockage, and radar networking. JTECH, 31, 599-619.

Tang, L., J. Zhang, C. Langston, J. Krause, K. Howard, and V. Lakshmanan, 2014: A physically based precipitation-nonprecipitation radar echo classifier using polarimetric radar and environmental data in a real-time system. Wea. Forecasting, 29, 1106-1119.

Wang, Y., P. Zhang, A. Ryzhkov, J. Zhang, and P.-L. Chang, 2014: Utilization of specific attenuation for tropical rainfall estimation in complex terrain. J. Hydromet. 15, 2250-2266.

Zhang, J., K Howard, C. Langston, et al., 2016: Multi-Radar Multi-Sensor (MRMS) Quantitative Precipitation Estimation: Initial Operating Capabilities. *Bull. Amer. Met. Soc.*, **97**, 621-638.